



**HAL**  
open science

# Influence of SiC reinforcement particles on the tribocorrosion behaviour of AlSiCp FGMs in 0.05M NaCl solution

a C Vieira, L A Rocha, Stéphane Mischler

► **To cite this version:**

a C Vieira, L A Rocha, Stéphane Mischler. Influence of SiC reinforcement particles on the tribocorrosion behaviour of AlSiCp FGMs in 0.05M NaCl solution. *Journal of Physics D: Applied Physics*, 2011, 44 (18), pp.185301. 10.1088/0022-3727/44/18/185301 . hal-00614339

**HAL Id: hal-00614339**

**<https://hal.science/hal-00614339>**

Submitted on 11 Aug 2011

**HAL** is a multi-disciplinary open access archive for the deposit and dissemination of scientific research documents, whether they are published or not. The documents may come from teaching and research institutions in France or abroad, or from public or private research centers.

L'archive ouverte pluridisciplinaire **HAL**, est destinée au dépôt et à la diffusion de documents scientifiques de niveau recherche, publiés ou non, émanant des établissements d'enseignement et de recherche français ou étrangers, des laboratoires publics ou privés.

1  
2  
3  
4  
5 **Influence of SiC reinforcement particles on the tribocorrosion**  
6 **behaviour of Al-SiC<sub>p</sub> FGM's in 0.05M NaCl solution**

7  
8  
9 A. C. Vieira<sup>1\*</sup>, L.A. Rocha<sup>1</sup>, S. Mischler<sup>2</sup>

10 <sup>1</sup> Centre for Mechanical and Materials Technologies (CT2M) and Department of Mechanical Engineering, University of Minho, Azurém,  
11 4800-058 Guimarães, Portugal

12 <sup>2</sup> Ecole Polytechnique Fédérale de Lausanne (EPFL), Tribology and Interface Chemistry Group, 1015 Lausanne, Switzerland

13 Received Date Line (to be inserted by Production) (8 pt)  
14  
15

---

16  
17 **Abstract**

18  
19 The main aim of this work was to study and understand the influence of SiC particles on the corrosion and  
20 tribocorrosion of Al matrix composite materials. For that, Al-SiC<sub>p</sub> functionally graded composites were produced  
21 by centrifugal casting and different SiC<sub>p</sub> contents were achieved. Their mechanical properties were improved by  
22 age-hardening heat-treatments. The tribocorrosion behaviour was studied in 0.05M NaCl solutions using a  
23 reciprocating motion tribometer involving an alumina ball sliding against the Al based samples. Above critical  
24 SiC particles content the matrix alloy surface was found protected against wear by SiC particles protruding from  
25 the surface. Below this threshold content, the SiC reinforcement was inefficient and the wear rate of the composite  
26 was the same as the non reinforced alloy.

27  
28 *Keywords:* Al alloy/SiC<sub>p</sub> composites, FGM, tribocorrosion

---

29  
30  
31 **1. Introduction**

32  
33 A functional graded material (FGM) can be defined as a material with two or more phases,  
34 which varies in some spatial direction its composition and/or microstructure. **The concept of**

---

\*Corresponding author. Tel.: +351 253 510 220; fax: +351 253 516 007.  
E-mail address: catarina.vieira@engmateriais.eng.uminho.pt (Ana Catarina Vieira)

1 composite material may be used to design FGM's, taking benefit of an inhomogeneous  
2 distribution of the reinforcing phase (metallic, ceramic or polymeric) resulting in an  
3 improvement of mechanical, thermal, electromagnetic, biochemical or biomechanical  
4 properties [1, 2-7]. For instances, by using centrifugal casting, SiC particles can be dispersed in  
5 an Al-based matrix with a graded distribution originating an Al-SiC<sub>p</sub> FGM [8,9]. Therefore, it  
6 is possible to combine surface hardness and high wear resistance with high bulk toughness  
7 [10].

8 In fact, Al-SiC<sub>p</sub> FGM's, have shown a great potential for several industries [10,11], being  
9 their major applications in electronic packaging industry, brake rotor assemblies or pistons  
10 rings in automotive industries and turbine components or rocket nozzles (relatively high-  
11 temperature environments) for advanced aircrafts and aerospace vehicles [1,12-15].

12 Because of the relatively good corrosion properties of aluminium, Al-SiC<sub>p</sub> FGM's are  
13 candidate materials for tribocorrosion applications where contact is exposed to the combined  
14 degradation by wear and corrosion. Examples of such tribocorrosion applications are chemical  
15 pumps, piston rings, cylinder walls and components in marine structures [16-18]. However,  
16 relatively little is known about the corrosion and tribocorrosion behaviour of aluminium based  
17 FGM's.

18 The reinforcement by SiC particles can influence the corrosion behaviour of the Al matrix.  
19 Preferential attack at the reinforcement/matrix interface (due to Al<sub>4</sub>C<sub>3</sub> formation at the  
20 interface), creation of local cathodes on conductive SiC catalysing the reduction of oxygen  
21 and/or modifications of the matrix alloy microstructure (alteration of the size and distribution  
22 of intermetallic phases) during composite production were phenomena reported in the literature  
23 as having influence on the corrosion resistance of Al-SiC<sub>p</sub> composites [16,19,20]. Clearly,  
24 these effects are highly dependent on the nature of the matrix Al alloy, on the SiC particles and  
25 on the heat treatments.

26 Also, the tribocorrosion behaviour of the material appears to be determined by the area  
27 fraction of reinforcement, particle mean size and tribological testing parameters. A. Velhinho  
28 et al [11] investigated the tribocorrosion behaviour of Al-SiC<sub>p</sub> functionally graded composites  
29 against cast iron pins in water using a unidirectional pin on disk tribometer. Two volume  
30 fractions (12.6 and 35.7%) of SiC particles with median size of 118 µm were considered.  
31 Those authors reported that the presence of water facilitated catastrophic SiC particle pull-out,

1 and therefore significantly increased wear. **Indeed, higher volume fractions of SiC particles**  
2 **were found to cause larger wear.** On the other hand, J.R. Gomes et al [21] **also studied** Al-SiC<sub>p</sub>  
3 functionally graded composites but using different experimental conditions: reciprocating  
4 sliding and a normal load of 10N. **Tests were conducted by using** cast iron pins counterfaces in  
5 a 3% NaCl solution and SiC particles area fraction varying between 25.8% and 33.4%. **In this**  
6 **case,** the wear rate of the composites was not significantly affected by the presence of the  
7 aqueous solution. **In contrast to Velhinho et al [11] results, higher amounts of reinforcement**  
8 **lead to lower wear rates. This behaviour was attributed to the capability of the SiC particles to**  
9 **anchor protective tribolayers and to their load-supporting effect allowing the protection of the**  
10 **Al matrix, contributing to a lower total wear of the composite material.**

11 C.-K. Fang et al [16] studied the synergistic effects of wear and corrosion for Al<sub>2</sub>O<sub>3</sub>  
12 particulate-reinforced 6061 Al matrix composites and postulated that, although the  
13 incorporation of reinforcement **was detrimental to the corrosion resistance of the material,** its  
14 influence on wear-corrosion was favourable. Therefore there is still a need for a mechanistic  
15 understanding of the involved phenomena.

16 This study aim was to gain a better understanding of the tribocorrosion mechanisms of Al-  
17 SiC<sub>p</sub> functionally graded composites. For this a model system consisting in Al-SiC<sub>p</sub> samples  
18 sliding against inert alumina balls in 0.05M NaCl was investigated. Aluminium matrix  
19 composites materials with a gradient in SiC content were fabricated using centrifugal casting.  
20 Samples of different SiC contents were obtained by machining the composite ingots in  
21 different locations. Heat treatments were carried out in order to improve the mechanical  
22 properties of the matrix. The corrosion mechanisms were evaluated using immersion and  
23 electrochemical techniques. During tribocorrosion the OCP was recorded in order to gain  
24 information on the prevailing mechanisms.

25

## 26 **2. Experimental details**

### 27 *2.1 Materials*

28

29 A non-commercial Al-10Si-4.5Cu-2Mg (wt. %) was selected as matrix of the composite.  
30 The alloy was home-developed in order to present specific properties, such as good castability  
31 (by adding Si), heat-treatment capability (by adding Cu) and good wettability (by adding Mg).

1 As reinforcement, SiC particles with 37.6  $\mu\text{m}$  as grain size distribution (10% of volumetric  
2 fraction) were selected. The functionally graded materials (FGM) were processed by  
3 centrifugal casting, using radial geometry, with 1500 rpm centrifugal speed.

4 Two different post-processing age hardening heat-treatments were made: solution treatment  
5 at 500 °C (2h and 8h), followed by quenching, plus an artificial aging at 160 °C during 512  
6 min. The solution treatments were made **in air**, in tubular furnace, while the artificial aging was  
7 made in a thermostatic silicone bath (Model Haake F6).

8 In this paper the samples solution treated during 2h were identified as FGM-S2h while the  
9 samples solution treated during 8h were identified as FGM-S8h. To use as reference, a non  
10 heat-treated sample was also studied and was identified as FGM-NHT.

11 The FGM microstructure was characterised using XRD (Cu  $K\alpha$  radiation, **continuous Bragg**  
12 **Brentano mode**, scan step size of 0.02°, Bruker D8 Discover equipment), SEM/EDS (Nano-  
13 SEM FEI Nova 200), and optical microscopy.

14 The particle area fraction was estimated by image analysis. For that, 25 to 30 images were  
15 acquired in an optical microscope and subsequently analysed with computer aided image  
16 analysis (Image tool 3.0).

17 Macro Vickers hardness measurements (30 Kg, 20s dwell time) were performed on all  
18 samples.

19

## 20 *2.2 Corrosion tests*

21

22 The samples were machined from the centrifugal cast-ring, in order to test the most exterior  
23 zone of the ring. Previous to each corrosion test, the samples were wet-polished up to 1200  
24 mesh in SiC abrasive paper.

25 The electrochemical solution used was 0.05M NaCl (pH = 6.2). The pH was measured  
26 before and after the corrosion tests. No variation in the pH was detected during the tests.

27 Two types of tests were carried out: immersion tests (to characterize localized corrosion  
28 mechanisms) and potentiodynamic polarization measurements (polarization curves). In the first  
29 tests, the samples were immersed in the solution (open circuit conditions) during 30 min and  
30 afterwards the corroded samples were analysed by SEM. Regarding the polarization curves, a

1 potential sweep rate of 0.5 mV/s in the noble direction (starting from cathodic values) was  
2 used. The samples were stabilized in the solutions during 1h before these measurements. A  
3 three-electrode electrochemical cell configuration integrating a standard double wall glass cell  
4 was used: a standard calomel reference electrode (SCE), a Pt counter electrode and the FGM  
5 samples connected as working electrode (WE) to the potentiostat (Autolab PGSTAT 30 under  
6 GPES software). In this paper, all potentials are given with respect to SCE.

### 8 *2.3 Tribocorrosion tests*

10 Disks were machined from the most exterior part of the centrifugal cast-ring, with  $\varnothing = 20$   
11 mm (+/- 0.1 mm) and 5 mm (+/- 0.1) thick. Previous to each test, the samples were polished  
12 down to 3  $\mu\text{m}$  diamond spray (from Struers). **The surface roughness ( $R_a$ ) was measured after**  
13 **polishing.  $R_a$  was of  $0.21 \pm 0.07 \mu\text{m}$  in the FGM samples.  $R_a$  values of the unreinforced**  
14 **centrifuged Al matrix was of  $0.04 \pm 0.01 \mu\text{m}$ .**

15 The tribocorrosion experiments were performed using the solution described above. The pH  
16 was evaluated before and after tribocorrosion tests to verify that no changes occurred during  
17 rubbing. The tests were done at OCP conditions in a reciprocating ball-on-plate tribometer  
18 (ball sliding against a stationary working electrode), with 1Hz frequency, 4 mm stroke length,  
19 11.4 mm/s as sliding velocity and 4N as normal applied load (at approximately 22 °C and  
20 relative humidity of 40%). The counterbody was an alumina ball ( $\varnothing = 6$  mm). Details on the  
21 tribometer used in the present study can be found elsewhere [22,23].

22 An electrochemical cell was mounted on the tribometer with a three electrodes  
23 configuration. The FGM sample was connected to a Wenking LB 95 L potentiostat as working  
24 electrode. A Pt counter electrode and a standard calomel reference electrode completed the  
25 electrochemical set-up.

26 The profiles of the wear tracks were quantified using non-contact scanning laser  
27 profilometry (UBM Telefokus instrument). Three profiles across the wear track for each  
28 sample were measured. The wear volume was calculated by multiplying the depth mean values  
29 by the track's length (4 mm) and by the width.

1 The worn surfaces were analysed by SEM/EDS. EDS spectra were obtained under an  
2 acceleration voltage of 15 KeV. The SEM/EDS equipment used were a Nano-SEM model –  
3 FEI Nova 200.

### 4 5 **3. Results**

#### 6 *3.1 Materials microstructural characterization*

7  
8 The FGM-NHT, FGM-S2h and FGM-S8h microstructural characterization was made by  
9 XRD and SEM, previous to corrosion and tribocorrosion tests. From the XRD pattern,  
10 presented in Figure 1, FGM-NHT, FGM-S2h and FGM-S8h samples presented the same  
11 phases:  $\alpha$ -Al, Si,  $\theta$  ( $\text{Al}_2\text{Cu}$ ), Q ( $\text{Al}_4\text{Cu}_2\text{Mg}_8\text{Si}_7$ ),  $\pi$  ( $\text{Al}_8\text{Si}_6\text{Mg}_3\text{Fe}$ ) and SiC. The first five phases  
12 were from the Al-matrix [24], being SiC the reinforcement phase.

13 The microstructures of FGM-NHT, FGM-S2h and FGM-S8h are presented in Figure 2. No  
14 significant differences can be observed between the samples, being the only dissimilarity  
15 related with the whitest phase identified by EDS as the Cu-rich phase  $\theta$ - $\text{Al}_2\text{Cu}$  [24]. In Figure  
16 2d) an EDS spectra obtained on the  $\theta$ - $\text{Al}_2\text{Cu}$  phases from the FGM-NHT sample is presented,  
17 confirming the presence of Al and Cu. Similar spectra were obtained in FGM-S2h and FGM-  
18 S8h samples. The heat treatment on the FGM samples leads to more fine and dispersed Cu-rich  
19 phases. From our previous work [24], the distribution and size of the Q- $\text{Al}_4\text{Cu}_2\text{Mg}_8\text{Si}_7$  and the  
20  $\pi$ - $\text{Al}_8\text{Si}_6\text{Mg}_3\text{Fe}$  phases on Al matrix alloys was shown to be not affected by the heat-  
21 treatments. On the other hand, the  $\theta$ - $\text{Al}_2\text{Cu}$  and Si phases becomes more fine and dispersed  
22 after the heat-treatment, being the decrease in size of the  $\theta$ - $\text{Al}_2\text{Cu}$  phase confirmed by image  
23 analysis.

24  
25 Table 1 lists the SiC particle area fraction as determined by image analysis. The hardness  
26 values of each sample are also presented in Table 1. Hardness increases with increasing SiC  
27 particle area fraction. This correlation was already reported in previous works [10,25].

28 Regarding the hardness mean values presented in Table 1, the lower hardness values were  
29 obtained in FGM-NHT (samples without heat-treatment), while the highest values were  
30 obtained with the FGM-S2h and FGM-S8h heat-treated samples.

### 3.2 Corrosion behaviour

The surface morphology of FGM-NHT sample, after immersion tests, is presented in Figure 3. There is preferential dissolution of the Al matrix around the  $\theta$ -Al<sub>2</sub>Cu phases (Figure 3a), by the formation of a galvanic couple between the Cu-rich phases (preferential cathodes) and the surrounding Al matrix (preferential anodes). This mechanism was confirmed as the main corrosion mechanism presented in the Al alloy matrix [24]. From Figure 3b), no preferential attack at the reinforcement/matrix interface as well as preferential dissolution of Al matrix around the SiC reinforcement particle can be noticed. Therefore, no effect of SiC reinforcement particles on the corrosion mechanisms can be suggested. This shows that SiC reinforcement does not alter, in the present conditions, the **corrosion mechanisms** of these Al alloys. Similar behaviour was observed in FGM-S2h and FGM-S8h samples when immersed in NaCl solution.

Figure 4 presents the potentiodynamic polarisation curves of the FGM samples in NaCl solution. For comparison, the polarization curve obtained with unreinforced Al matrix (without SiC reinforcement particles) is also presented. The reproducibility of the tests being very good, only one curve per condition was plotted. No significant differences can be detected between the different samples.  $E_{\text{corr}}$  is similar to all the samples ( $\approx -0.60\text{V}$ ). Therefore, in NaCl solution, apparently, neither the presence of SiC particles nor the heat-treatment does significantly influence the corrosion behaviour of the material.

### 3.3 Tribocorrosion behaviour

The evolution of the open circuit potential (OCP) with time during tribocorrosion testing of FGM-NHT, FGM-S2h and FGM-S8h samples of different SiC particle contents are presented in Figure 5a), Figure 5b) and Figure 5c), respectively. Each test was identified in accordance with the SiC particle area fraction value presented on the tested sample surface. **For comparison, the results obtained with unreinforced Al matrix samples (without SiC<sub>p</sub> and identified in the figures with 0%) are also presented.** Before rubbing, the corrosion potential values are similar in all the samples (approximately  $-0.6\text{V}$ ). The OCP decreases when rubbing

1 starts. This behaviour is usually attributed to the breaking of the passive film on the wear track  
2 area by the abrading alumina ball [17, 26-28]. Once rubbing stops depassivation ceases and the  
3 potential recovers its initial value.

4 During rubbing, between 1200s and 1800s, samples without SiC and samples with lower  
5 SiC particles area fraction values, have OCP values in the range of -0.9V to -1.0V. This trend  
6 indicates that during rubbing, the material surface is being constantly depassivated. However,  
7 for higher SiC particles area fraction values (for instances,  $23 \pm 4$  % in Figure 5a), after the  
8 initial cathodic shift, the OCP recovers during rubbing reaching the value observed before  
9 sliding, suggesting that repassivation of the sample surface occurred during rubbing.

10 In case of repassivation occurring during rubbing, a correlation between the evolution of  
11 OCP and friction coefficient with time was observed (Figure 6a), where negative peaks in OCP  
12 corresponds to positive peaks in friction coefficient. When repassivation did not occur during  
13 rubbing, the coefficient of friction attained more stable values within short time (Figure 6b).  
14 This behaviour was observed systematically in heat-treated samples as well on the non heat-  
15 treated material.

16 The wear volume estimated after the tribocorrosion samples are presented as a function of  
17 the SiC particles area fraction in Figure 7. For comparison data, the unreinforced alloys [22]  
18 are also plotted. The SiC reinforcement does not affect significantly wear volume values up to  
19 a volume fraction of approximately 15% above which a steady decrease in wear is observed.  
20 The minimum wear volume values were achieved to volume fraction similar or higher than  
21 18%. The low wear volumes exhibited by FGM-S2h and FGM-S8h samples are likely due to  
22 the increase in hardness induced by the heat treatment.

23 Two typical wear patterns were observed using SEM. The first one corresponds to heat  
24 treated and non heat treated samples with SiC contents lower or equal to 15% where large  
25 plastic flow and material smearing characterise the worn surface (Figure 8a). The two large pits  
26 (approximately 30  $\mu\text{m}$ ) observed in Figure 8a) are likely due to the pull out of SiC particles.  
27 The second characteristic pattern is observed on samples with SiC contents higher than 18%.  
28 These samples present a more corrugated topography with visible SiC particles (Figure 8b)  
29 protruding from the surface as shown in the magnified micrograph shown in Figure 8c) and  
30 Figure 8d). Between 15% and 18% of SiC particle area fraction, intermediate mechanisms  
31 were observed.

1 Rubbing induced surface transformations in the contacting area of the alumina balls as  
2 shown in Figure 9. The transformation consisted in crystallographic etching of the surface and  
3 an area of a layer partially covering the ball. This layer was material transferred from the  
4 composite counter body. EDS analysis revealed the presence of Al, Cu, Si and Mg but not of  
5 SiC (Z1 and Z2 in Figure 9b). **Although the detected Al** could be attributed both to the alumina  
6 ball and to the Al matrix alloy, the presence of Si, Cu and Mg strongly suggested the presence  
7 of the metallic matrix in the alumina surface. Regarding Z3 zone from Figure 9b), only Al and  
8 O elements were identified, indicating that, in this zone, only alumina is present.

#### 10 **4. Discussion**

11  
12 Two main mechanisms usually contribute to material degradation in the tribocorrosion of  
13 passive metals: wear-accelerated corrosion and mechanical wear [17,29]. The latter mechanism  
14 involves the mechanical removal of metallic particles by counter-body asperities or trapped  
15 third body particles digging below the metal surface. Wear-accelerated corrosion arises from  
16 the fact that an asperity rubbing on a metal surface produces a track of clean metal which is  
17 usually more sensitive to corrosion than the original metal protected by a thin oxide film  
18 (passive film). In the present case, the cathodic shift of the potential observed at the onset of  
19 rubbing (Figure 5) reveals that depassivation and thus wear-accelerated corrosion occur. When  
20 rubbing stops the potential recovers its initial (before rubbing) value. For samples with the  
21 highest SiC particle area fraction values, the potential recovery occurs already during rubbing  
22 indicating that depassivation ceased. This particular effect can be explained by the appearance  
23 of reinforcement SiC particles standing proud of the aluminium matrix surface (Figure 8c).  
24 These protruding SiC particles limit or even suppress direct contact between the metal and the  
25 alumina ball as schematically illustrated in Figure 10a). In such situation, depassivation of the  
26 aluminium matrix is not expected to occur and thus the wear track recovers the passive state of  
27 the surrounding areas and the galvanic coupling effect disappears. For the lowest SiC particle  
28 area fraction contents the direct metal/ball contact (Figure 10b) is maintained during the entire  
29 rubbing period as indicated by the observed stable cathodic potential shift and the absence on  
30 protruding SiC particles. Furthermore, strong wear action on the matrix can lead to pull-out of

1 SiC particles that loose the mechanical support of the surrounding matrix, as shown in Figure  
2 8a).

3 Figure 11 summarizes the observations concerning the passivity recovery during rubbing as  
4 a function of heat treatment and SiC content. All samples with a SiC content of 18% or higher  
5 exhibit passivity recovery during rubbing. This threshold concentration corresponds well with  
6 the SiC content above which protruding reinforcement particles are observed in the wear  
7 tracks. It also corresponds to the SiC content above which wear significantly decreases (Figure  
8 7). Clearly, protruding particles not only limits plastic deformation (Figure 8) and thus  
9 depassivation but they also protect against wear. Interestingly, below 18% the wear intensity is  
10 not affected by the presence of SiC reinforcement, the composite materials exhibiting the same  
11 wear rate as the un-reinforced alloys.

12 The data obtained here do not permit drawing conclusions about the possible influence of  
13 heat treatment on the threshold SiC content for wear transition. More experiments with  
14 reinforcement contents around 18% are needed to obtain statistically relevant results.  
15 Nevertheless the heat treatment has a clear effect on the overall wear rate. In particular, before  
16 the transition, wear is more severe on the non heat-treated alloy probably due to the lower  
17 hardness of the metal matrix.

18 The two situations depicted in Figure 10 may also explain the correlation found between the  
19 coefficient of friction and the corrosion potential (Figure 6). Indeed, when plastic flow occurs,  
20 depassivation is large and thus the potential attains very negative values. This situation  
21 corresponds to a direct contact of the alumina counter ball (covered with transferred material)  
22 and the composite metal and thus to a specific frictional interaction. When SiC particles  
23 protrudes from the surface the contact is established between these particles and the counter  
24 resulting in a different frictional force and the reduction in plastic deformation of the metal  
25 matrix and thus of the cathodic shift of the corrosion potential. The SiC-counter ball contact  
26 (Figure 10a) produces less friction than the metal matrix one (Figure 10b). This can be  
27 explained by the smooth appearance of the protruding SiC particles and by the suppression of  
28 large plastic deformation they induce.

29

## 30 **5. Conclusions**

31

1 The corrosion and tribocorrosion behavior of Al-SiC<sub>p</sub> FGM's in 0.05M NaCl was  
2 investigated using samples obtained by centrifugal casting and therefore, presenting different  
3 SiC contents in the most exterior part of the tested surfaces. The conclusions of this study are:

- 4 - The introduction of SiC particles and heat-treatments do not affect the corrosion  
5 behavior of the composite materials. The polarization curves follow similar trends with  
6 or without reinforcement particles.
- 7 - Two tribocorrosion mechanisms observed were depending on SiC<sub>p</sub> content: above 18%  
8 the SiC particles were found protruding from the surface and thus protecting the  
9 surrounding metal matrix against wear and wear accelerated corrosion. Below 18% the  
10 SiC particles had no effect on wear and generalized plastic flow, larger wear and wear  
11 accelerated corrosion characterized the FGM's wearing surfaces.

### 13 **Acknowledgements**

14 The research team was financially supported by the Portuguese Foundation for Science and  
15 Technology (FCT – Portugal) under a PhD scholarship (SFRH / BD / 27911 / 2006). The  
16 authors thank also to Dr.<sup>a</sup> Edith Ariza (University of Minho) and Pierre Mettraux (EPFL) for  
17 SEM analysis.

### 19 **References**

- 20 [1] M.M. Gasik, Industrial applications of FGM solutions, *Materials Science Forum*, 423  
21 (2003) 17-22.
- 22 [2] T. Ogawa, Y. Watanabe, H. Sato, I. Kim, Y. Fukui, Theoretical study on fabrication of  
23 functionally graded material with density gradient by a centrifugal solid-particle method,  
24 *Composites Part A: Applied Science and Manufacturing*, 37 (2006) 2194-2200.
- 25 [3] N.B. Duque, Z.H. Melgarejo, O.M. Suarez, Functionally graded aluminum matrix  
26 composites produced by centrifugal casting, *Materials Characterization* 55 (2005) 167-171.
- 27 [4] S. El-Hadad, H. Sato, E. Miura-Fujiwara, Y. Watanabe, Fabrication of Al-Al<sub>3</sub>Ti/Ti<sub>3</sub>Al  
28 functionally graded materials under a centrifugal force - Review, *Materials*, 3 (2010) 4639-  
29 4656.

- 1 [5] D. Lin, Q. Li, W. Li, S. Zhou, M.V. Swain, Design optimization of functionally graded  
2 dental implant for bone remodeling, *Composites: Part B* 40 (2009) 668–675.
- 3 [6] F. Watari, A. Yokoyama, M. Omori, T. Hirai, H. Kondo, M. Uo, T. Kawasaki,  
4 Biocompatibility of materials and development to functionally graded implant for bio-medical  
5 application, *Composites Science and Technology* 64 (2004) 893-908.
- 6 [7] H. Hassanin, K. Jiang, Functionally graded microceramic components, *Microelectronic*  
7 *Engineering* 87 (2010) 1610-1613.
- 8 [8] Y. Watanabe, A. Kawamoto, K. Matsuda, Particle size distributions in functionally graded  
9 materials fabricated by the centrifugal solid-particle method, *Composites Science and*  
10 *Technology* 62 (2002) 881-888.
- 11 [9] Y. Watanabe, N. Yamanaka, Y. Fukui, Control of composition gradient in a metal ceramic  
12 functionally graded material manufactured by the centrifugal method, *Composites Part A* 29A  
13 (1998) 595-601.
- 14 [10] A.C. Vieira, P.D. Sequeira, J.R. Gomes, L.A. Rocha, Dry sliding wear of Al alloy/SiC<sub>p</sub>  
15 functionally graded composites: Influence of processing conditions, *Wear* 267 (2009) 585-592.
- 16 [11] A. Velhinho, J. D. Botas, E. Ariza, J.R. Gomes, L. A. Rocha, Tribocorrosion Studies in  
17 Centrifugally Cast Al-matrix SiC<sub>p</sub>-reinforced Functionally Graded Composites, *Materials*  
18 *Science Forum* 456 (2004) 871-875.
- 19 [12] J.W. Gao, C.Y. Wang, Modeling the solidification of functionally graded materials by  
20 centrifugal casting, *Materials Science and Engineering A*292 (2000) 207-215.
- 21 [13] S. Uemura, The activities of FGM on new applications, *Materials Science Forum*, 423  
22 (2003) 1-10.
- 23 [14] L.L. Mishnaevsky Jr., Functionally gradient metal matrix composites: Numerical analysis  
24 of the microstructure–strength relationships, *Composites Science and Technology*, 66 (2006)  
25 1873-1887.
- 26 [15] Y. Miyamoto, W.A. Kaysser, B.H. Rabin, A. Kawasaki, R.G. Ford, *Functionally graded*  
27 *materials: Design, processing and applications*, Kluwer Academic Publishers, 1999.
- 28 [16] C.-K. Fang, C.C. Huang, and T.H. Chuang, Synergistic effects of wear and corrosion for  
29 Al<sub>2</sub>O<sub>3</sub> particulate–reinforced 6061 aluminium matrix composites, *Metallurgical and Materials*  
30 *Transactions*, 30A (1999) 643.

- 1 [17] S. Mischler, Triboelectrochemical techniques and interpretation methods in  
2 tribocorrosion: A comparative evaluation, *Tribology International* 41 (2008) 573-583.
- 3 [18] D. Landolt, S. Mischler, M. Stemp, Electrochemical methods in tribocorrosion: a critical  
4 appraisal, *Electrochimica Acta* 46 (2001) 3913-3929.
- 5 [19] M. Montoya-Dávila, M.I. Pech-Canul, M.A. Pech-Canul, Effect of SiC<sub>p</sub> multimodal  
6 distribution on pitting behaviour of Al/SiC<sub>p</sub> composites prepared by reactive infiltration,  
7 *Powder Technology* 195 (2009) 196-202.
- 8 [20] A. Pardo, M.C. Merino, S. Merino, F. Viejo, M. Carboneras, R. Arrabal, Influence of  
9 reinforcement proportion and matrix composition on pitting corrosion behaviour of cast  
10 aluminium matrix composites (A3xx.x/SiC<sub>p</sub>), *Corrosion Science* 47 (2005) 1750-1764.
- 11 [21] J.R. Gomes, A.R. Ribeiro, A.C. Vieira, A.S. Miranda and L.A. Rocha, Wear mechanisms  
12 in functionally graded aluminium matrix composites: Effect of the presence of an aqueous  
13 solution, *Materials Science Forum* 493 (2005) 33-38.
- 14 [22] A.C. Vieira, L.A. Rocha, S. Mischler, Mechanical and electrochemical deterioration  
15 mechanisms in the tribocorrosion of Al alloys in NaCl and in NaNO<sub>3</sub> solutions, Accepted in  
16 *Corrosion science* (2010).
- 17 [23] J. Stojadinovic, D. Bouvet, M. Declercq, S. Mischler, Effect of electrode potential on the  
18 tribocorrosion of tungsten, *Tribology International* 42 (2009) 575-58.
- 19 [24] A.C. Vieira, A.M. Pinto, L.A. Rocha, S. Mischler, Effect of Al<sub>2</sub>Cu precipitates size and  
20 mass transport on the polarization behavior of age-hardened Al-Si-Cu-Mg alloys in 0.05 M  
21 NaCl, *Electrochim. Acta* (2011) doi:10.1016/j.electacta.2011.02.044.
- 22 [25] D.P. Mondal, S. Das, High stress abrasive wear behavior of aluminum hard particle  
23 composites: Effect of experimental parameters, particle size and volume fraction, *Tribology*  
24 *International* 39 (2006) 470-478.
- 25 [26] P. Ponthiaux, F. Wenger, D. Drees, J.P. Celis, Electrochemical techniques for studying  
26 tribocorrosion processes, *Wear* 256 (2004) 459-468.
- 27 [27] D.E. Taylor, R.B. Waterhouse, An electrochemical investigation on fretting corrosion of a  
28 number of pure metals in 0.5M sodium chloride, *Corrosion Science* 14 (1974) 111-122.
- 29 [28] B. Bethune, R.B. Waterhouse, Electrochemical studies of fretting corrosion, *Wear* 12  
30 (1968) 27-34.
- 31 [29] D. Landolt, *Corrosion and Surfaces Chemistry of Metals*, 1<sup>st</sup> ed., EPFL Press, 2007.

1 **List of Figures:**

2

3 **Figure 1.** XRD patterns obtained in the Al-SiC<sub>p</sub> FGM-NHT, FGM-S2h and FGM-S8h  
4 samples.

5

6 **Figure 2.** SEM micrographs obtained in backscattering electron mode (BE mode) of: a) FGM-  
7 NHT; b) FGM-S2h; c) FGM-S8h; d) EDS spectra obtained on the  $\theta$  phases presented in FGM-  
8 NHT sample.

9

10 **Figure 3.** SEM micrographs obtained in FGM-NHT sample after immersion tests of 30 min in  
11 0.05M NaCl solution (backscattering electron mode): a) Identification of  $\theta$ -Al<sub>2</sub>Cu phases; b)  
12 Identification of SiC particles. Similar micrographs were identified in FGM-S2h and in FGM-  
13 S8h samples.

14

15 **Figure 4.** Polarisation curves of FGM-NHT, FGM-S2h, FGM-S8h and unreinforced Al matrix  
16 samples, in 0.05M NaCl solution.

17

18 **Figure 5.** Corrosion potential evolution with time during the tribocorrosion tests in: a) FGM-  
19 NHT; b) FGM-S2h; c) FGM-S8h samples tested in 0.05M NaCl solution. Each test is  
20 identified in accordance with the SiC particle area fraction value presented on the sample  
21 surface.

22

23 **Figure 6.** Friction coefficient and corrosion potential evolution during the tribocorrosion tests  
24 in 0.05M NaCl, for: a) FGM-NHT with  $23 \pm 4\%$  SiC; b) FGM-S2h with  $14 \pm 6\%$  SiC;

25

26 **Figure 7:** Relation between the wear volume values measured after tribocorrosion tests and the  
27 SiC particle area fraction values of FGM-NHT, FGM-S2h and FGM-S8h samples in 0.05M  
28 NaCl.

29

1 **Figure 8.** SEM micrographs obtained after the tribocorrosion tests in 0.05M NaCl solution in  
2 the wear track of FGM-NHT sample with: a) SiC<sub>p</sub> particle area fraction of  $15 \pm 3\%$  **obtained in**  
3 **secondary electron mode (SE mode)**; b) SiC<sub>p</sub> particle area fraction of  $23 \pm 4\%$ , (SE mode); c)  
4 **and d) SiC<sub>p</sub> particle area fraction of  $23 \pm 4\%$ , (BE mode; 40° tilted).**

5  
6 **Figure 9:** SEM micrographs obtained in the alumina counterbody after the tribocorrosion tests  
7 in 0.05M NaCl tested with the FGM-NHT sample (SE mode).

8  
9 **Figure 10:** Schematic representation of two wear mechanisms suggested: a) Mechanical  
10 contact between the protruded SiC reinforcement particles and the Al<sub>2</sub>O<sub>3</sub> counterbody; b)  
11 Mechanical contact between the Al matrix and the Al<sub>2</sub>O<sub>3</sub> counterbody.

12  
13 **Figure 11:** Relation between the potential values measured 100s before stopping rubbing (at  
14 1700s) and the SiC particle area fraction values of FGM-NHT, FGM-S2h and FGM-S8h  
15 samples tested in 0.05M NaCl. Black symbols represent the situation where potential recover  
16 during rubbing was observed.

17

1 **List of Tables:**

2

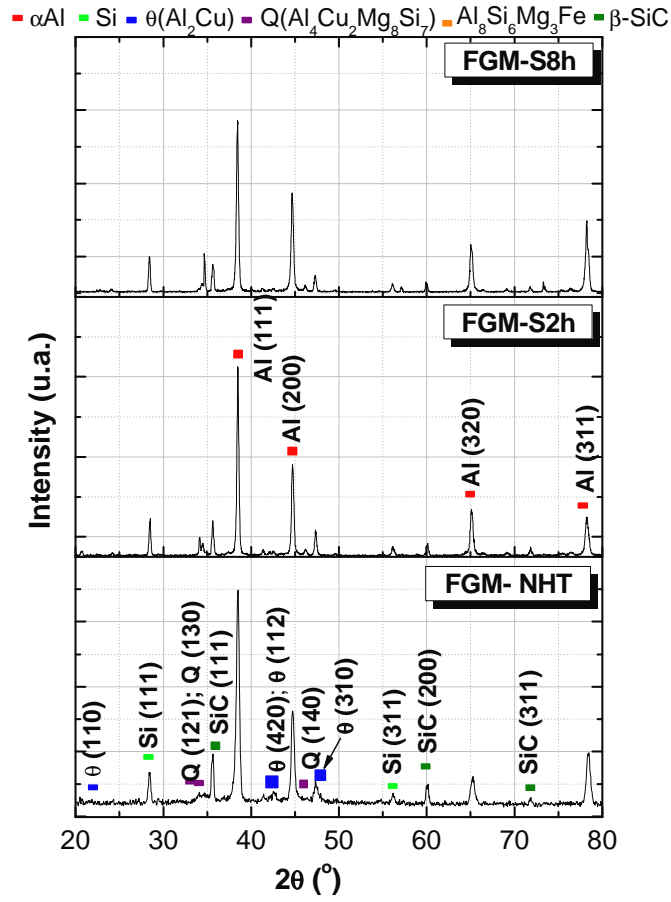
3 **Table 1.** Characterization of the samples tested in the tribocorrosion tests in 0.05M NaCl  
4 solution, regarding the SiC particle area fraction on the surface sample and macro Vickers  
5 hardness (HV<sub>30</sub>).

6

7

1 **Figure 1.**

2

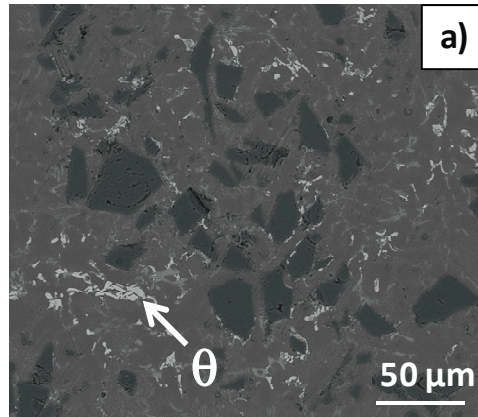


3

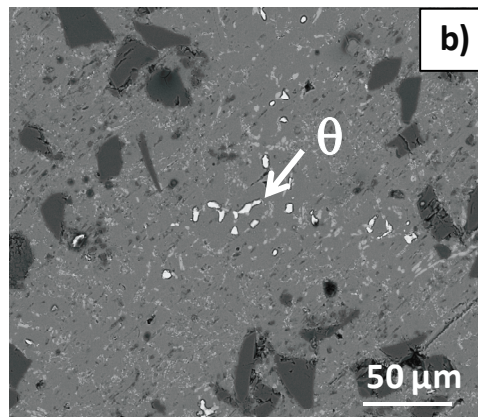
4

1 **Figure 2**

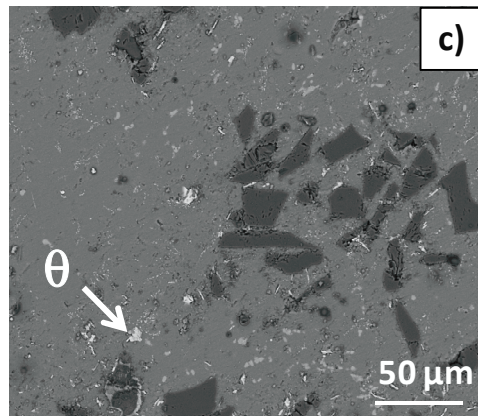
2



3

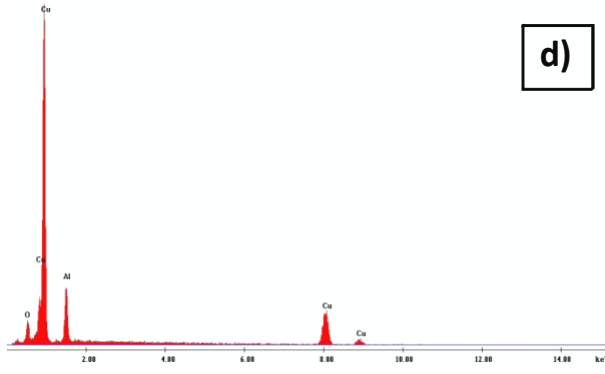


4



5

d)



1  
2

1 **Figure 3**

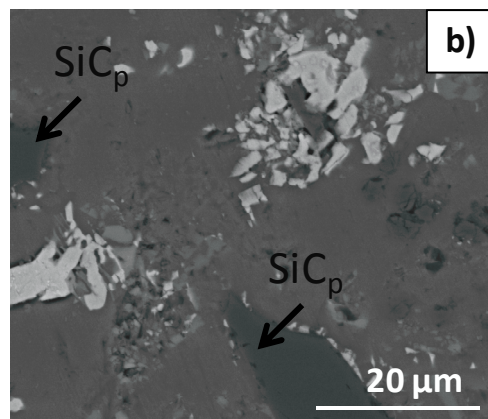
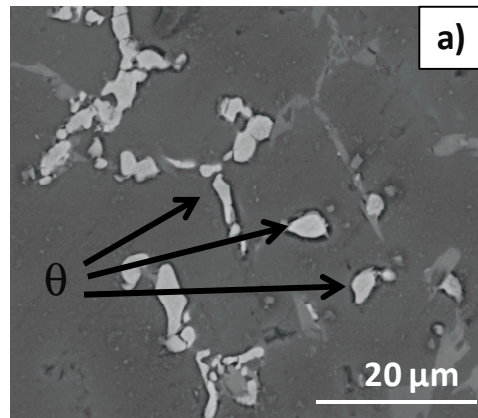
2

3

4

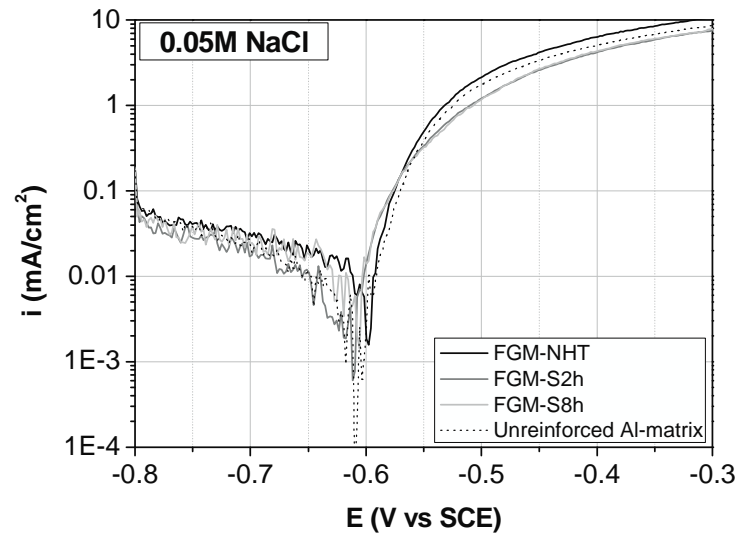
5

6



1 **Figure 4**

2

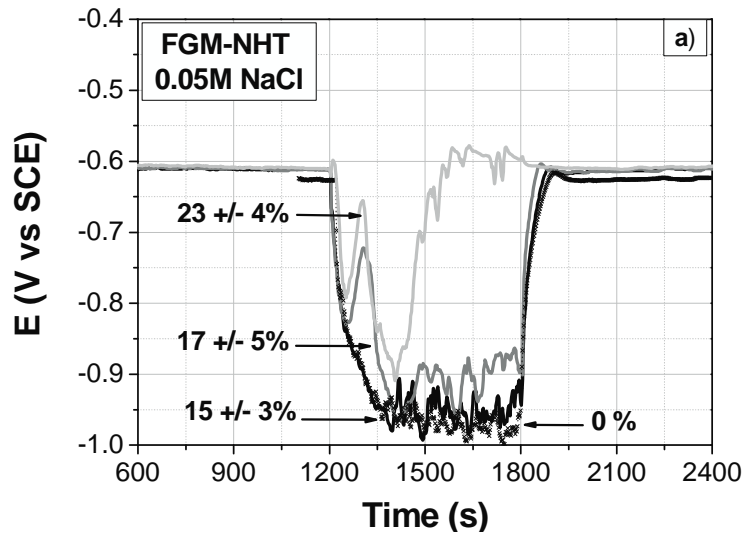


3

4

1 **Figure 5**

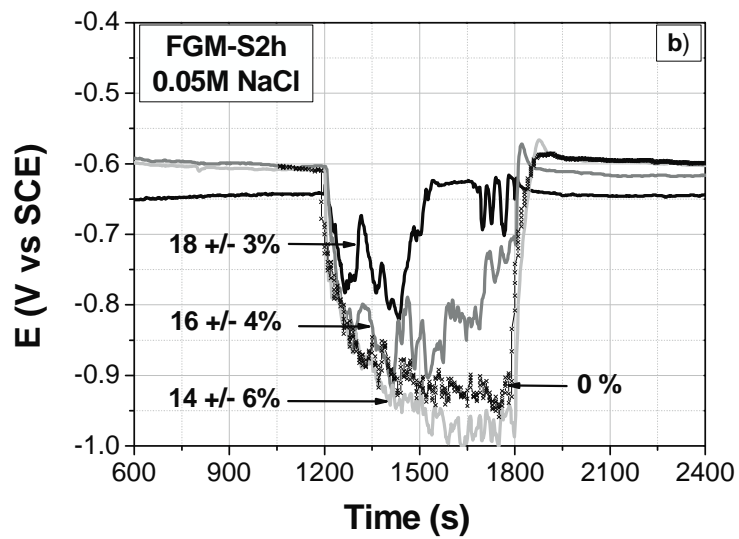
2



3

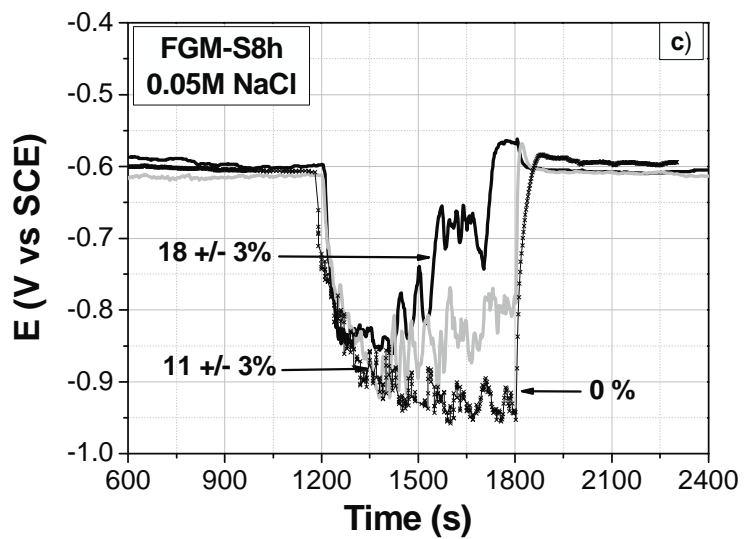
4

5



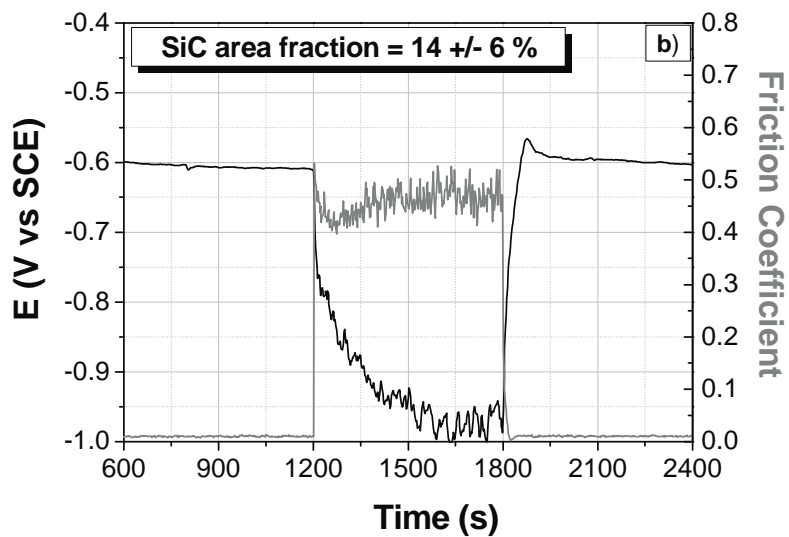
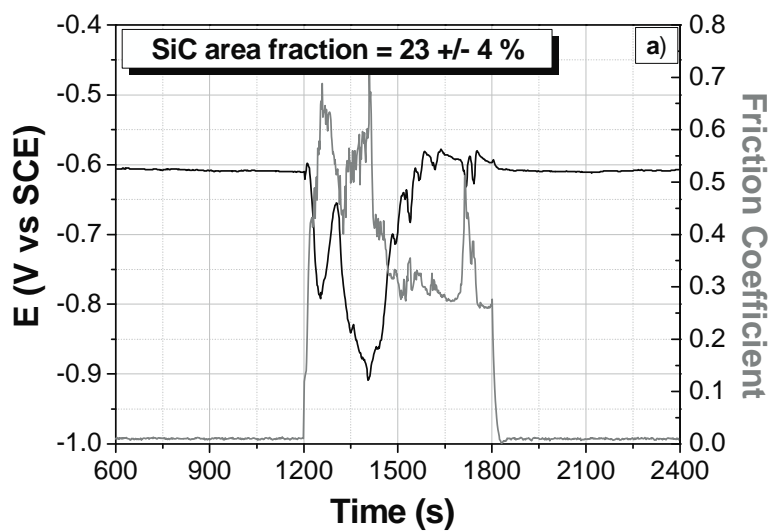
6

7



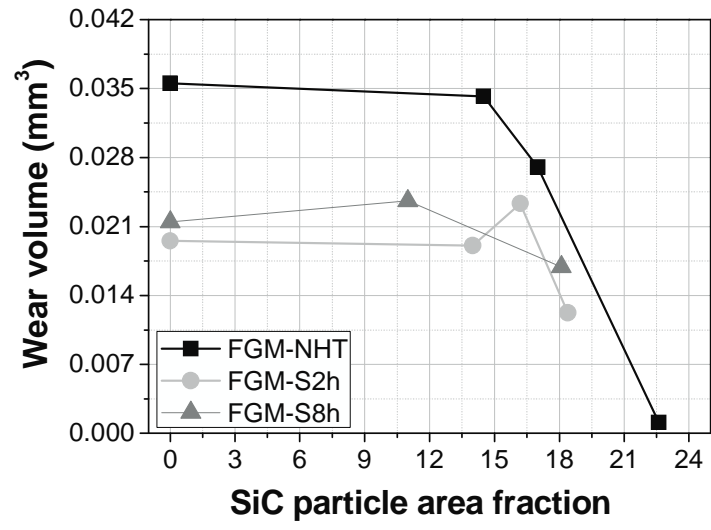
1  
2

Figure 6



1 **Figure 7**

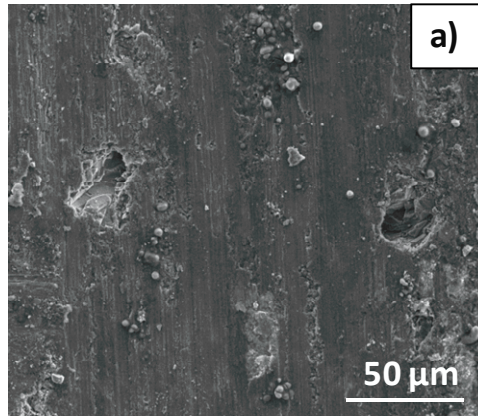
2  
3



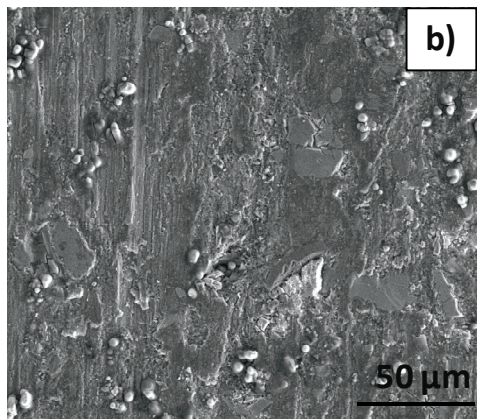
4  
5

1 **Figure 8**

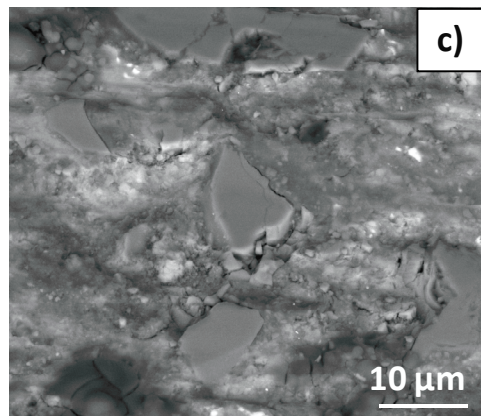
2  
3



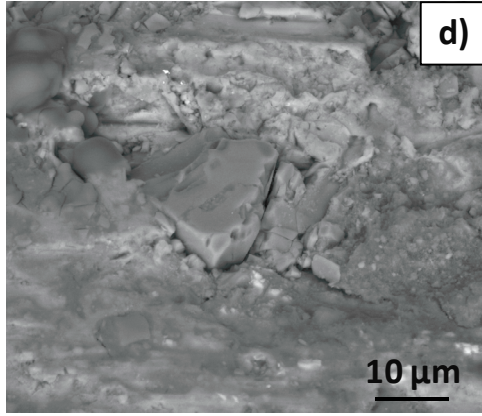
4  
5



6  
7

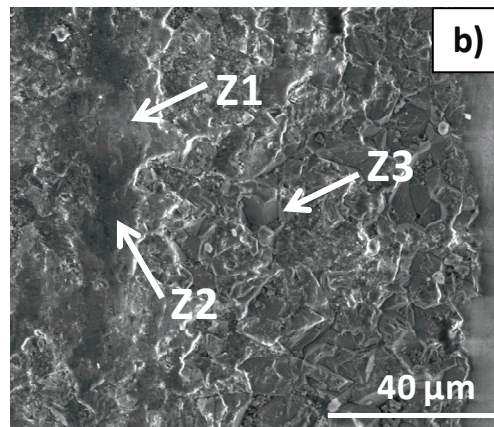
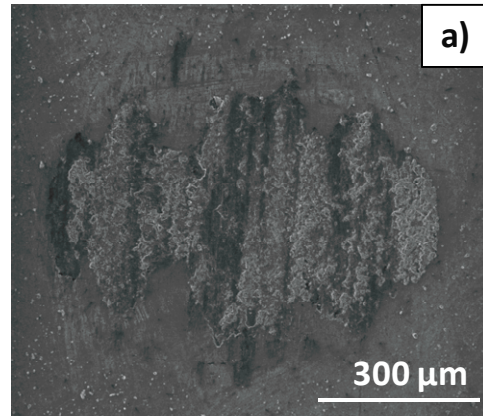


1  
2



1 **Figure 9**

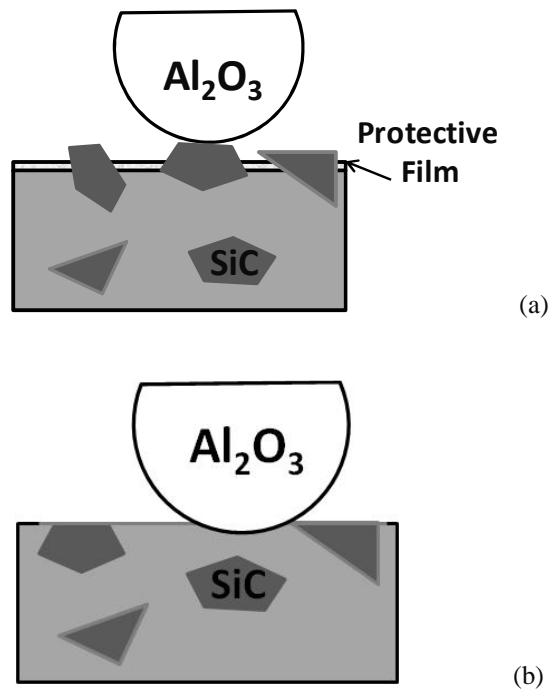
2  
3



5  
6

1 **Figure 10**

2

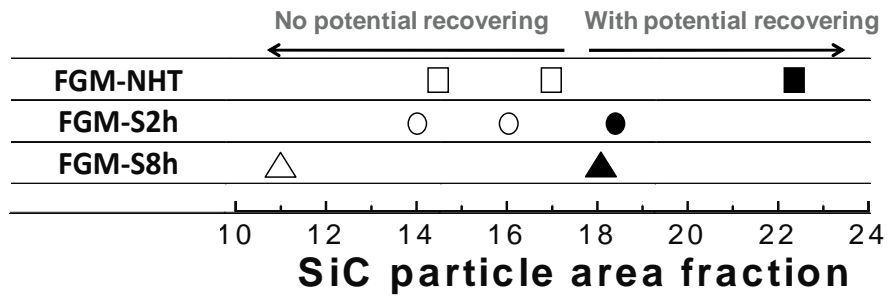


3

4

1 **Figure 11**

2



3

4

1 **Table 1**

2

	<b>SiC particle area fraction (%)</b>	<b>HV<sub>30</sub></b>	<b>HV<sub>30</sub> (mean values)</b>
<b>FGM - NHT</b>	$15 \pm 3$	$135 \pm 6$	$140 \pm 18$
	$17 \pm 5$	$141 \pm 3$	
	$23 \pm 4$	$159 \pm 13$	
<b>FGM- S2h</b>	$14 \pm 6$	$176 \pm 4$	$179 \pm 10$
	$16 \pm 4$	$180 \pm 6$	
	$18 \pm 3$	$189 \pm 11$	
<b>FGM- S8h</b>	$11 \pm 3$	$180 \pm 0$	$177 \pm 9$
	$18 \pm 3$	$181 \pm 6$	

3

4

5

6